

Parton coalescence and the antiproton/pion anomaly at RHIC

V. Greco,¹ C. M. Ko,¹ and P. Lévai^{1,2}

¹*Cyclotron Institute and Physics Department, Texas A&M University, College Station, Texas 77843-3366, USA*

²*KFKI Research Institute for Particle and Nuclear Physics, P.O. Box 49, Budapest 1525, Hungary*

(Dated: February 9, 2020)

Coalescence of minijet partons with the partons from the quark-gluon plasma formed in relativistic heavy ion collisions is suggested as the mechanism for production of hadrons with intermediate transverse momentum. The resulting enhanced antiproton and pion yields at intermediate transverse momentum gives a plausible explanation for the observed large antiproton to pion ratio. With further increasing momentum, the ratio is predicted to decrease and approach the small value given by independent fragmentations of minijet partons after their energy loss in the quark-gluon plasma.

PACS numbers: 25.75.-q, 25.75.Dw, 25.75.Nq, 12.38.Bx

Heavy ion collisions at the Relativistic Heavy Ion Collider (RHIC) provides the possibility of creating in the laboratory a plasma of deconfined quarks and gluons. One of the signatures for the quark-gluon plasma (QGP) is suppression of jet production [1]. Experimental data on high transverse momentum hadrons [2, 3], which are dominantly produced from the minijet partons originated from the initial hard processes between colliding nucleons, have indeed shown a large suppression compared to what is expected from the superposition of primary binary nucleon-nucleon collisions. The amount of energy loss of minijet partons, particularly gluons, is consistent with the scenario that they have traversed through a dense matter that consists of colored quarks and gluons [4, 5]. The mechanism for the formation of high transverse momentum hadrons from the minijet partons is usually modeled by fragmentation functions which describe how minijet partons combine with the quarks and antiquarks from the vacuum to form hadrons as they separate. The parameters in the fragmentation functions can be determined by fitting the experimental data from high energy electron-positron annihilation and proton-proton collisions. Because of the presence of the quark-gluon plasma, which is lacking in proton-proton collisions, minijet partons in heavy ion collisions can also combine with the quarks and antiquarks in the QGP to form hadrons. Since the average momenta of quarks and antiquarks in the QGP are much smaller than those of minijet partons, these hadrons have momenta between those from the independent fragmentations of minijet partons and from the hadronization of the QGP. These intermediate momentum hadrons thus carry information about the QGP formed in relativistic heavy ion collisions.

In this letter, we shall adopt the coalescence model to study the formation of hadrons from minijet partons with the QGP partons. The coalescence model has previously been used in the ALCOR [6] and MICOR [7] models to describe the hadron yield from the QGP expected to be formed in relativistic heavy ion collisions. More recently, it has been introduced in a Multiphase Transport Model (AMPT) [8] to model the hadronization of

the partonic matter formed during the initial stage of relativistic heavy ion collisions [9]. Coalescence of hard minijet partons with soft QGP partons was first introduced in Ref. [10] to predict the flavor ordering of the elliptic flow of high transverse momentum hadrons. In the present study, we shall show that including hadrons from this production mechanism besides thermal hadrons from the hadronization of an expanding QGP can explain the increasing antiproton to pion ratio at low transverse momentum and comparable antiproton and pion yields at intermediate transverse momentum observed in recent experimental data from RHIC [11]. We further show that the antiproton to pion ratio decreases at large transverse momenta and approaches the small value given by the independent fragmentations of minijet partons.

We consider central Au+Au collisions (0 – 10%) at 200 AGeV. The transverse momentum distribution of minijet partons in the midrapidity can be obtained from an improved perturbative QCD calculation [12] with the parton distribution function of a nucleon in the nucleus Au including a transverse momentum smearing. Kinematic details and a systematic analysis of pp collisions can be found in Ref. [12]. Using the GRV94 LO result for the PDF [13] and the KKP fragmentation function from Ref. [14], the measured data in the reaction $pp \rightarrow \pi^0 X$ at $\sqrt{s} = 200$ GeV can be reproduced with an average transverse momentum smearing of 1.4 GeV. To include parton energy loss in the QGP formed in the collisions, we use an effective opacity $L/\lambda = 3.5$ as extracted from fitting the spectrum of high transverse momentum pions measured at RHIC [5].

Taking the momentum cutoff $p_0 = 1.75$ GeV/c for the minijet partons, the transverse momentum spectra of minijet partons at midrapidity ($y = 0$) in central Au+Au collisions at $\sqrt{s} = 200$ AGeV are shown in Fig. 1 for the gluon (dash-dotted curve), u (solid curve) and \bar{u} (dashed curve) quarks. The d and \bar{d} quark distributions are similar to those of u and \bar{u} quarks.

The QGP partons, which dominate transverse momentum below p_0 , are taken to have a temperature $T = 180$ MeV and to occupy a volume $V = 730$ fm³. This thermal

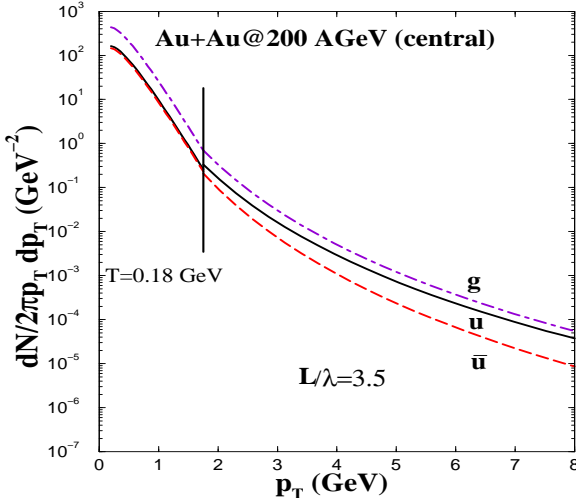


FIG. 1: Parton transverse momentum distributions at hadronization in Au+Au collisions at $\sqrt{s} = 200$ AGeV. The minijet partons with transverse momentum greater than 1.75 GeV/c after energy loss are shown by dash-dotted curve for gluons, solid curve for u quarks, and dashed curve for \bar{u} quarks. Partons with transverse momentum below 1.75 GeV/c are from the quark-gluon plasma at temperature $T = 180$ MeV.

parton transverse momentum distribution is also shown in Fig. 1. Compared to the power-like minijet parton spectrum, the spectrum of thermal partons is exponential. Because of scattering of minijet partons with the thermal partons as they traverse the QGP, those with momentum around p_0 are expected to be thermalized with the QGP partons, leading to a smooth spectrum around p_0 . In the present schematic study, we neglect this effect. The total transverse energy per unit rapidity given by the thermal and minijet partons is about 570 GeV and is consistent with that measured in experiments. Most of this transverse energy comes from soft thermal partons as the contribution of minijet partons is only about 10%.

The basic equation in the coalescence model for the formation of a pion from a quark and an antiquark is similar to that for deuteron production from nucleons [15, 16, 17] and can be written as

$$\frac{dN_\pi}{d^3\mathbf{p}_\pi} = g_\pi \int d^3\mathbf{x}_1 d^3\mathbf{x}_2 d^3\mathbf{p}_1 d^3\mathbf{p}_2 f_q(\mathbf{x}_1, \mathbf{p}_1) f_{\bar{q}}(\mathbf{x}_2, \mathbf{p}_2) \times \delta^3(\mathbf{p}_\pi - \mathbf{p}_1 - \mathbf{p}_2) f_\pi(\mathbf{x}_1 - \mathbf{x}_2, \mathbf{p}_1 - \mathbf{p}_2). \quad (1)$$

In the above, $f_q(\mathbf{x}, \mathbf{p})$ and $f_{\bar{q}}(\mathbf{x}, \mathbf{p})$ are the Wigner distribution functions for quarks and antiquarks, respectively, and they are normalized to their numbers, i.e., $\int d^3\mathbf{x} d^3\mathbf{p} f_{q,\bar{q}}(\mathbf{x}, \mathbf{p}) = N_{q,\bar{q}}$. The Wigner function for the pion is denoted by $f_\pi(\mathbf{x}, \mathbf{p})$, and it is normalized as $\int d^3\mathbf{x} d^3\mathbf{p} f_\pi(\mathbf{x}, \mathbf{p}) = (2\pi)^3$. The factor g_π takes into account the probability of forming a colorless spin zero pion from the spin 1/2 color quarks, e.g., $g_{\pi^+} = 1/36$ for forming a π^+ from a pair of u and \bar{d} quarks.

Assuming that quarks and antiquarks are uniformly distributed in the fireball of volume V , then the quark and antiquark Wigner functions are simply related to their momentum distributions, i.e., $f_{q,\bar{q}}(\mathbf{x}, \mathbf{p}) = 1/V dN_{q,\bar{q}}/d^3\mathbf{p}$. The Wigner function of pion depends on the spatial and momentum distributions of its constituent quark and antiquark. For a schematic study, we use uniform distributions, i.e.,

$$f_\pi(\mathbf{x}, \mathbf{p}) = \frac{9\pi}{2\Delta_x^3 \Delta_p^3} \Theta(\Delta_x - |\mathbf{x}|) \Theta(\Delta_p - |\mathbf{p}|), \quad (2)$$

where Δ_x and Δ_p are, respectively, the spatial and momentum cutoff in the phase space of the quark-antiquark relative motion. The value of Δ_x should be about the size of pion, while that of Δ_p should be larger than \hbar/Δ_x due to the uncertainty relation.

For hadrons in the midrapidity ($y = 0$), we only need to consider their transverse momentum. Also, we generally expect that the minijet partons are essentially massless while the thermal partons are massive due to nonperturbative effects. Since we are mainly interested in hadrons with relatively large momenta, and they are chiefly formed from the coalescence of relative high momentum partons, we take the thermal partons to be massless for simplicity. In this case, partons move with speed of light, so only comoving partons, i.e., moving in the same direction, can coalescence to form hadrons. This leads to the following simplified expression for coalescence of quarks and antiquarks to form pions:

$$\begin{aligned} \frac{dN_\pi}{d^2\mathbf{p}_{\pi,T}} = & g_\pi \frac{6\pi^2 \Delta_x^3}{V p_{\pi,T}} \int p_{q,T} dp_{q,T} p_{\bar{q},T} dp_{\bar{q},T} \\ & \times \frac{dN_q}{d^2\mathbf{p}_{q,T}} \frac{dN_{\bar{q}}}{d^2\mathbf{p}_{\bar{q},T}} \delta(p_{\pi,T} - p_{q,T} - p_{\bar{q},T}) \\ & \times \Theta(\Delta_p - |p_{q,T} - p_{\bar{q},T}|/2). \end{aligned} \quad (3)$$

The above results can be generalized to formation of protons and antiprotons from the parton distribution functions. We take the antiproton Wigner function as

$$\begin{aligned} f_{\bar{p}}(\mathbf{x}, \mathbf{y}; \mathbf{p}, \mathbf{q}) = & \frac{9\pi}{2\Delta_x^3 \Delta_p^3} \Theta(\Delta_x - |\mathbf{x}|) \Theta(\Delta_p - |\mathbf{p}|) \\ & \times \frac{9\pi}{2\Delta_y^3 \Delta_q^3} \Theta(\Delta_y - |\mathbf{y}|) \Theta(\Delta_q - |\mathbf{q}|), \end{aligned} \quad (4)$$

where $\mathbf{x} = (\mathbf{x}_1 - \mathbf{x}_2)$ and $\mathbf{y} = (\mathbf{x}_1 + \mathbf{x}_2)/2 - \mathbf{x}_3$ are the relative coordinates among the three antiquarks, while $\mathbf{p} = (\mathbf{p}_1 - \mathbf{p}_2)/2$ and $\mathbf{q} = (\mathbf{p}_1 + \mathbf{p}_2 - \mathbf{p}_3)/2$ are the corresponding relative momenta. As for pions, uncertainty relation requires $\Delta_x \Delta_p$ and $\Delta_y \Delta_q$ cannot be less than \hbar . For simplicity, we take $\Delta_x = \Delta_y$ and $\Delta_p = \Delta_q$. This leads to the following antiproton transverse momentum

spectrum from coalescence of three partons:

$$\begin{aligned} \frac{dN_{\bar{p}}}{d^2\mathbf{p}_{\bar{p},T}} &= g_{\bar{p}} \frac{36\pi^4 \Delta_x^6}{V^2 p_{\bar{p},T}^2} \int \prod_{i=1,3} p_{\bar{q}_i,T} dp_{\bar{q}_i,T} \frac{dN_{\bar{q}_i}}{d^2\mathbf{p}_{\bar{q}_i,T}} \\ &\times \delta(p_{\bar{p},T} - p_{\bar{q}_1,T} - p_{\bar{q}_2,T} - p_{\bar{q}_3,T}) \\ &\times \Theta(\Delta_p - |p_{\bar{q}_1,T} - p_{\bar{q}_2,T}|/2) \\ &\times \Theta(\Delta_p - |p_{\bar{q}_1,T} + p_{\bar{q}_2,T} - p_{\bar{q}_3,T}|/2). \end{aligned} \quad (5)$$

In the above, $g_{\bar{p}}$ is the probability of forming a colorless spin 1/2 antiproton from three antiquarks, e.g., $g_{\bar{p}} = 1/108$ for forming an antiproton from two \bar{u} quarks and one \bar{d} quark.

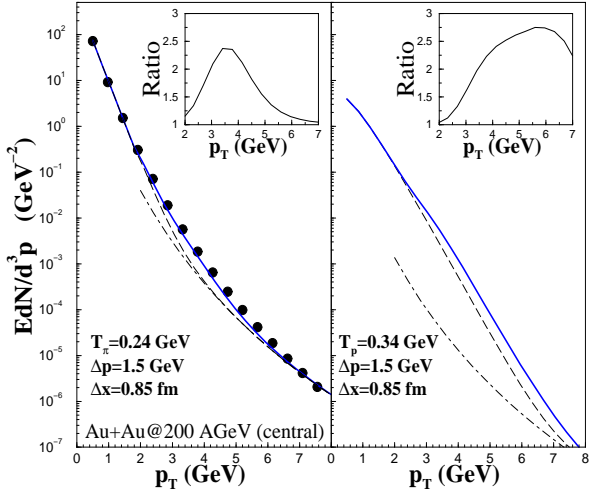


FIG. 2: Transverse momentum spectra of pions (left panel) and antiprotons (right panel) from Au+Au collisions at $\sqrt{s} = 200$ AGeV. Dashed curves are results including contributions from thermal hadrons and hadrons from independent fragmentations of minijet partons (dash-dotted curves). Adding also hadrons from coalescence of minijet partons with QGP partons gives the solid curves. Ratio of the solid to the dashed curve is given in the insets. Experimental data from the PHENIX Collaboration on the π^0 spectrum [18] are shown by filled circles.

We first take thermal hadrons to have exponential transverse mass ($m_T = \sqrt{m^2 + p_T^2}$) spectra with inverse slope parameter equal to 240 MeV for pions and 340 MeV for antiprotons in order to reproduce the observed low transverse momentum spectra of these particles. The larger inverse slope parameter than the QGP temperature reflects the effect due to collective transverse flow of the QGP, which increases the transverse momentum of heavier antiprotons more than that of lighter pions. The number of thermal pions is fixed by fitting the measured pion spectrum at low transverse momentum, while that of thermal antiprotons is determined by requiring that it is 0.7 of the pion number at transverse momentum of 2 GeV/c as in experimental measurements. Hard hadrons, shown in Fig. 2 by dash-dotted curves, are obtained from minijet partons using the KKP fragmentation function of Ref. [14], which has been shown to reproduce the mea-

sured high transverse momentum particles at RHIC. The hadron spectra from the sum of these two contributions are shown in Fig. 2 by dashed curves. As shown in the left panel, the final pion spectrum at intermediate transverse momentum is below the experimental data from the PHENIX Collaboration [18] shown by filled circles.

To evaluate the contribution to pion and antiproton production from coalescence of minijet quarks and antiquarks with those from the QGP, the effect due to gluons is taken into account by converting them to quark-antiquark pairs with equal probability for different flavors as assumed in the ALCOR model [6]. Using $\Delta_p = 1.5$ GeV/c and $\Delta_x = 0.85$ fm for pion, the coalescence contribution leads to a final pion spectrum, shown by the solid curve in the left panel of Fig. 2, that agrees with the experimental data. The large value of Δ_p can be contributed to the fact that the relative momentum between the quark and antiquark in a pion increases with its velocity in the partonic matter. For simplicity, the same Δ_p and Δ_x are used to evaluate the coalescence contribution to antiproton production, and the resulting final antiproton spectrum is shown by the solid curve in the right panel of Fig. 2. From the ratio of hadron spectra with and without the coalescence contribution shown in the insets in Fig. 2, this new mechanism is seen to enhance the yields of intermediate transverse momentum pions and antiprotons by a factor of about 2.5.

In Fig. 3, we show the ratio of antiproton to pion as a function of transverse momentum obtained with different scenarios for the antiproton spectrum but the same empirical pion spectrum shown in the left panel of Fig. 2. The dashed curve corresponds to an antiproton spectrum that includes only the thermal and perturbative ones, i.e., the dashed curve in the right panel of Fig. 2. This theoretical result is below the experimental antiproton to pion ratio given by filled squares [11] when the transverse momentum is above 2 GeV/c. Including antiproton production from the coalescence of minijet partons with thermal partons enhances the ratio significantly as shown by the dashed curve with open circles, which is now above the experimental ratio.

Since the collective flow effect is expected to diminish with increasing antiproton transverse momentum, we explore this possibility by varying the inverse slope parameter of the transverse momentum spectrum of thermal antiprotons above 2.5 GeV/c. Taking the inverse slope parameter of these antiprotons to be 240 MeV, same as that for pions, the antiproton to pion ratio is shown in Fig. 3 by the dash-dotted curve and the dash-dotted curve with open circle for the cases without and with the coalescence contribution to antiproton production, respectively. In this case, coalescence of minijet and QGP partons again increases appreciably the antiproton to pion ratio at intermediate transverse momentum compared to that without this contribution, bringing the theoretical results closer to the experimental data. If the

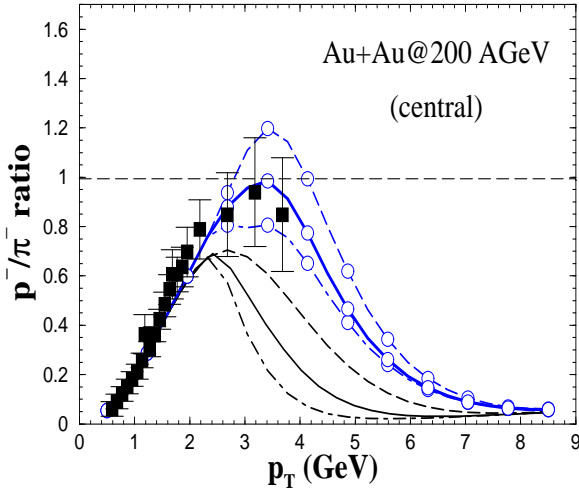


FIG. 3: Antiproton to pion ratios from Au+Au collisions at $\sqrt{s} = 200$ AGeV. Dash-dotted, solid, and dashed curves are results using, respectively, 240, 290, and 340 MeV for the inverse slope parameter of intermediate transverse momentum antiprotons. Corresponding results including also contributions from coalescence of minijet and QGP partons are shown with open circles. Filled squares are the experimental data [11].

inverse slope parameter of intermediate transverse momentum thermal antiprotons is taken to have a value of 290 MeV, between those of low transverse momentum thermal pions and antiprotons, the resulting antiproton to pion ratio is shown by the solid curve and the solid curve with open circles in Fig. 3 for the cases without and with the coalescence contribution. It is seen that the experimental data can now be reproduced with the inclusion of antiproton production from the coalescence of minijet partons with thermal partons.

The antiproton to pion anomaly has previously been attributed to enhanced production of antiprotons with intermediate momentum from the baryon junctions in incident nucleons [19]. Recently, a parton recombination model similar to the coalescence model used here has also been used in Ref. [20] to explain the antiproton/pion anomaly by using a parton distribution function that is fitted to measured pion transverse momentum spectrum.

In summary, we have proposed a mechanism for the hadronization of minijet partons in heavy ion collisions at relativistic energies. Instead of the usual independent fragmentations, in which they combine with the quark-antiquark in the vacuum to form hadrons, these minijet partons are allowed to coalescence with thermal quarks and antiquarks from the quark-gluon plasma created in the collisions to form hadrons. Using the minijet partons predicted from the perturbative QCD, we find that this mechanism is important for production of hadrons with intermediate transverse momentum, leading to comparable antiproton and pion yields in this momentum region as observed experimentally. It further predicts that the antiproton to pion ratio would decrease as their transverse momenta become large. In this high transverse

momentum region, independent fragmentations of minijet partons dominate particle production and lead to a very small antiproton to pion ratio. Confirmation of this hadronization mechanism thus provides another evidence for the formation of the quark-gluon plasma in relativistic heavy ion collisions.

We are grateful to Su Hwang Lee for useful discussions. P.L. would also like to thank discussions with G. Papp and G. Fai, and the warm hospitality of the Cyclotron Institute at Texas A&M University during his visit. This work is based on work supported in part by the U.S. National Science Foundation under Grant No. PHY-0098805 and the Welch Foundation under Grant No. A-1358. The work of V.G. is further supported by a fellowship from the National Institute of Nuclear Physics (INFN) in Italy, while that of P.L. by Hungarian OTKA T034269 and T043455.

- [1] X. N. Wang, Phys. Rev. C 58, 2321 (1998).
- [2] K. Adcox *et al.* (PHENIX Collaboration), Phys. Rev. Lett. 88, 022301 (2002).
- [3] C. Adler *et al.* (STAR Collaboration), Phys. Rev. Lett. 89, 202301 (2002).
- [4] M. Gyulassy, P. Lévai, and I. Vitev, Phys. Rev. Lett. 85, 5535 (2000); Nucl. Phys. B 571, 197 (2000); *ibid.* B 594, 371 (2001); M. Gyulassy, I. Vitev, and X. N. Wang, Phys. Rev. Lett. 86, 2537 (2001).
- [5] P. Lévai *et al.*, Nucl. Phys. A 698, 631 (2002); M. Gyulassy, P. Lévai, and I. Vitev, Phys. Lett. B 538, 282 (2002).
- [6] T. S. Biró, P. Lévai, and Zimányi, Phys. Lett. B 347, 6, (1995); Phys. Rev. C 59, 1574 (1999); T. S. Biró, T. Csörgő, . P. Lévai, and Zimányi, *ibid.* B 472, 273 (2000).
- [7] P. Csizmadia and P. Lévai, Phys. Rev. C 61, 0301903 (2000); J. Phys. G 28, 1997 (2002).
- [8] B. Zhang *et al.*, Phys. Rev. C 61, 067901 (2000); *ibid.* 62, 054905 (2000); 65, 054909 (2002); Z. Lin *et al.*, *ibid.* 64, 011902 (2001); Nucl. Phys. A 498, 375c (2002).
- [9] Z. Lin and C. M. Ko, Phys. Rev. C 65, 034904 (2002); Z. Lin, C. M. Ko, and S. Pal; Phys. Rev. Lett. 89, 152301 (2002).
- [10] Z. Lin and C. M. Ko, Phys. Rev. Lett. 89, 202302 (2002).
- [11] K. Adcox, Phys. Rev. Lett. 88, 242301 (2002); T. Chujo, nucl-ex/209027; T. Sakagushi, nucl-ex/0209030.
- [12] Y. Zhang *et al.*, Phys. Rev. C 65, 034903 (2002).
- [13] M. Glück, E. Reya, and W. Vogt, Z. Phys. C 67, 433 (1995).
- [14] B.A. Kniehl, G. Kramer, and B. Pötter, Nucl. Phys. B 597, 337 (2001); hep-ph/0011155
- [15] C. Dover *et al.*, Phys. Rev. C 44, 1636 (1991).
- [16] A. J. Baltz and C. Dover, Phys. Rev. C 53, 362 (1996).
- [17] R. Mattiello *et al.* Phys. Rev. C 55, 1443 (1997).
- [18] D. d'Enterria for the PHENIX Collaboration, hep-ex/0209051.
- [19] I. Vitev and M. Gyulassy, Phys. Rev. C 65, 041902 (2002).
- [20] R. C. Hwa and C. B. Yang, nucl-th/0211010.